Visual
Abstract

Analysis of the structural integrity of a frozen wall during a mine shaft excavation using temperature monitoring data

Lev Levin, Mikhail Semin
Mining Institute of the Ural Branch of the Russian Academy of Sciences, Russia
aerolog_lev@mail.ru, https://orcid.org/0000-0003-0767-9207
seminma@inbox.ru, https://orcid.org/0000-0001-5200-7931

Ivan Golovatyi
Joint Stock Company "Belaruskali", Belarus
iwan15@yandex.by

ABSTRACT. The construction of shafts of potash mines in flooded and unstable soils is usually carried out with the help of artificial ground freezing. The freezing process aims to form a waterproof frozen wall (FW) around the shaft and is monitored throughout the construction of the mine shaft. This paper describes the results of the temperature monitoring of the FW around the skip shaft of a potash mine under construction. The data on temperature measurements in control-thermal boreholes were used to parameterize the mathematical model of heat transfer, which allowed for the reconstruction of the temperature field throughout the entire cooled and frozen soil volume. The resulting temperature distribution in the FW zone for greater than one year was used to determine the distribution of the strength properties and calculate the temporary change in the limiting value of the external lateral load on an FW of a given thickness and specified thermomechanical properties. The obtained dependencies of the maximum external load on the FW can be used to optimize the operation mode of the freezing station at the ice holding stage (or passive freezing) to increase the energy efficiency of the system and ensure the structural integrity of the FW.

KEYWORDS. Frozen wall, Artificial ground freezing, Mine shaft, Temperature monitoring, Structural integrity, Optimization of freezing parameters.

OPEN ACCESS

INTRODUCTION

The construction of mine shafts in flooded unstable soils is conducted using special methods. Regarding potash mines, the most common method for shaft construction is artificial ground freezing (AGF). Its purpose is to create a frozen wall (FW) around the designed mine shaft [1, 2].

The regulatory documentation in Belarus and many other countries require systematic monitoring of the FW state during the AGF process. In general, the monitoring consists of measuring the temperature along the depth of several vertical boreholes [3]. Based on the temperature distribution data, the engineer must judge whether the required FW thicknesses have been achieved. In general, this type of investigation is conducted based on an interpretation of the temperature field throughout the entire volume of cooled and frozen soil via back analysis [4] or by solving the inverse Stefan problems [5, 6]. Next, using the selected isotherm (0°C or lower), the actual FW thickness is determined and compared with the calculated thickness obtained from the preliminary mechanical analysis. When performing a mechanical analysis, it is generally assumed that the FW temperature is uniformly distributed throughout the volume of the frozen soils [7, 8]. Such an average temperature is equal to a predetermined negative value at which the strength properties of the soils were determined during laboratory tests. Additionally, this value is used to calculate the design FW thickness.

The advantage of this approach is associated with the speed of the assessment of the FW bearing capacity; however, this is based on simplifications, which in certain practical situations can be very rough [8]. Among them are the following:

− A change in the strength properties with a variation in the temperature.
− The thermal expansion of wet soils when the pore water freezes.
− Moisture bulging out of the area of the frozen soils, which leads to an increase in the external load on the side wall of the frozen soil cylinder.
− The influence of frost heaving on the stress-strain state of the FW.

All these factors are associated with the absence of the mutual influence of stress-strain and the thermal fields in the FW model. However, the literature has also described an alternative approach – the solution to coupled thermo-hydro-mechanical (THM) problems [9, 10]. This approach allows one to describe the physical processes in frozen soils more accurately; however, it has its disadvantages, for example, the duration of the simulation and the large amount of additional initial data required for it, the rheological and hydraulic parameters of the frozen soils at various temperatures, the frost heaving parameters, etc. This alternative approach has not been addressed in this paper.

Let us consider in more detail a consequence of neglecting the temperature changes in the mechanical and strength properties of the frozen soils in the first approach. The calculated FW thicknesses, determined from mechanical analysis based on the average uniform temperature of the FW, are typically satisfactory in practice at the ice growing stage (or active freezing). However, upon transition to the ice holding stage (or passive freezing), the power of the freezing system decreases. In this case, the zone of negative temperatures typically continues to expand, but the average temperature of the FW can increase significantly [11]. The latter is associated with an increase in the temperature of the brine in the freezing columns. Therefore, it becomes incorrect to compare the actual FW thicknesses along the same isotherm with the calculated FW thicknesses since, in this case, the thicknesses are compared for completely different average temperatures of the FW.

Even though the FW thickness (determined from the isotherm of the actual freezing of the pore water) continues to increase, the actual bearing capacity of the FW may decrease due to an increase in its average temperature. The FW bearing capacity can also become lower than the required value, which can lead to significant deformations of the unsupported shaft walls, and a flow of groundwater into the shaft. Thus, observations during the sinking of shafts No. 2 and No. 3 of the third Bereznikovsky potash mine [12] showed that during the transition from the ice growing stage to the ice holding stage, the temperature increased, and water inflows were often noted. With a significant increase in the temperature of the FW, holes containing thawed soils can form, through which groundwater will flow into the shaft.

The opposite situation can also occur when engineers slowly reduce the power of the freezing station when switching to the ice holding stage. This leads to the average temperature of the FW retaining its design values; however, simultaneously, the FW thickness continues to increase. It leads to over freezing of the soil volume and entails the inefficient use of the refrigeration capacity.

The above-mentioned scenarios indicate the importance of selecting the correct mode of operation of the freezing stations during the ice holding stage, considering the increasing average temperature of the FW. In this regard, it is necessary to solve an optimization problem associated with the selection of the growth rate the brine temperature in the freezing pipes, in which the bearing capacity of the FW (expressed, for example, in terms of the maximum lateral load on its side wall) will retain a constant value equal to the designed external load on the FW. To solve the optimization problem, we first must determine the method to calculate the dynamically changing bearing capacity of the FW according to the data of the field monitoring of the AGF process. The literature does not describe such methods that consider in sufficient detail the effect of the temperature field on the bearing capacity of the FW and at the same time allow performing quick analysis, without solving coupled THM problems. The existing methods for optimizing the AGF consider other aspects of this problem: the influence of seepage flows [13, 14], the common influence of brine parameters on the freezing rate [15], selective freezing [16], etc. The problem of determining the temperature of the brine at the stage of maintaining the FW thickness was considered only within the framework of the analysis of temperature fields [17].

This paper presents a practical case of AGF for the skip shaft of a potash mine under construction. Based on the soil temperature monitoring data, the temperature field was restored throughout the entire volume of cooled and frozen soils at various points in time. This temperature field was used to evaluate the evolution of the FW bearing capacity over time and draw conclusions regarding how optimal the selected freezing mode was. The purpose of this study was to describe and demonstrate the methodology for estimating the dynamically changing bearing capacity of the FW according to the experimental temperature monitoring of the AGF process.

OBJECT OF THE STUDY AND EXPERIMENTAL OBSERVATIONS DATA

The focus of this study was the frozen soils of the skip shaft of the Darasinsky potash mine, which was under construction. The mine is located in the Soligorsk district of the Minsk region in the Republic of Belarus. The difficult hydrogeological conditions of the shaft construction were associated with the presence of flooded loose and unstable soil layers in the upper part of the sedimentary cover, to a depth of 185 m. This predetermined the requirement to use AGF.

A total of 39 freeze pipes were installed around the designed skip shaft. The diameter of the freeze pipe contour was 15.4 m, and the distance between the mouths of the adjacent freeze pipes was approximately 1.24 m. The diameter of the designed mine shaft was 8 m (see Fig. 1).

In the present work, the dynamics of the bearing capacity of the FW was studied during the ice growing and ice holding stages. We obtained and processed the experimental data of temperature monitoring in three control-thermal (CT) boreholes located near the freeze pipe contour (see Fig. 1). The temperature measurements were obtained daily throughout the entire height of the CT boreholes (185 m) using the DTS system [18, 19]. Fig. 2 shows the typical temperature distributions along the CT borehole heights at various time points.
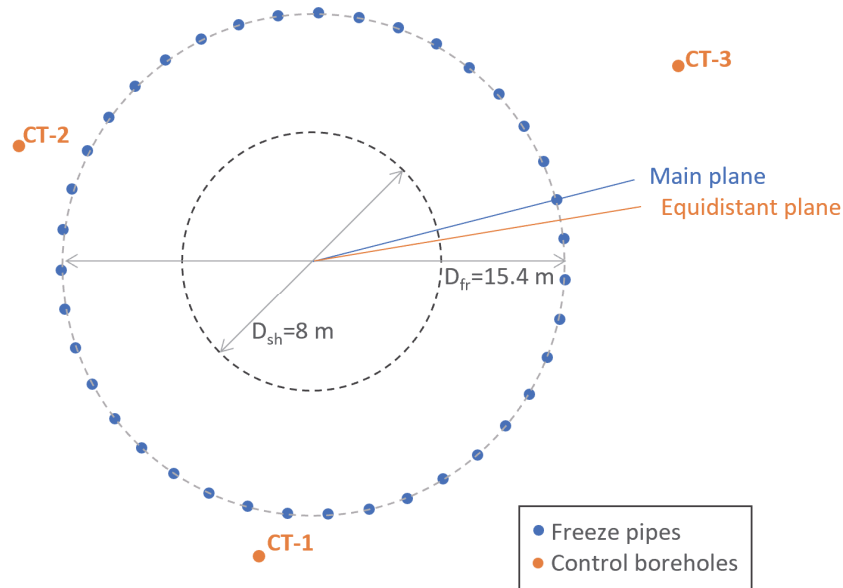
Figure 1: Locations of the freeze pipes and control-thermal boreholes of the skip shaft.

Over time, the temperature of the soils in the vicinity of the CT boreholes decreased. Moreover, this decrease occurred more rapidly, the closer the CT borehole was located to the freeze pipe contour. The non-uniformity of the temperature decrease along the height of each CT borehole was also noted. This was because, in the freezing interval, various soil layers existed that had significantly different thermophysical properties. The spatial temperature distributions in the CT boreholes were generally correlated with each other, except for a small zone at a depth of 140 m, where a local maximum was observed in CT-2, and a local minimum was observed in CT-3. This feature was associated with the groundwater seepage in the sandstone layer at this depth, which was described in detail in [20].

Fig. 3a shows the time dependencies of the brine temperature measured at the inlet and outlet of the freezing pipes. A decrease in the temperature of the incoming brine compared to the design values (from –25 to –23°C) occurred in the

interval from December 3 to December 19, 2022. Subsequently, the temperature gradually decreased until March 14, 2021. After that date, the temperature increased by 3°C, which was associated with the transition to the ice holding stage. Up until September 2021, the temperature gradually decreased, which was associated with natural processes in the soil. On September 8, the temperature again increased sharply by 2°C, which was associated with a change in the operation mode of the freezing station. The same sharp temperature increase occurred on October 28, 2021 and January 7, 2022.

The total brine flow rate in the brine pipe system during the entire freezing period under consideration also changed. In the initial period from November 25 to January 28, it varied in the range from 220 to 278 m³/hour, after which it was maintained at 260 m³/hour. From July 5, 2021, it decreased first to 210 m³/h, then to 180 and 160 m³/h (see Fig. 3b).
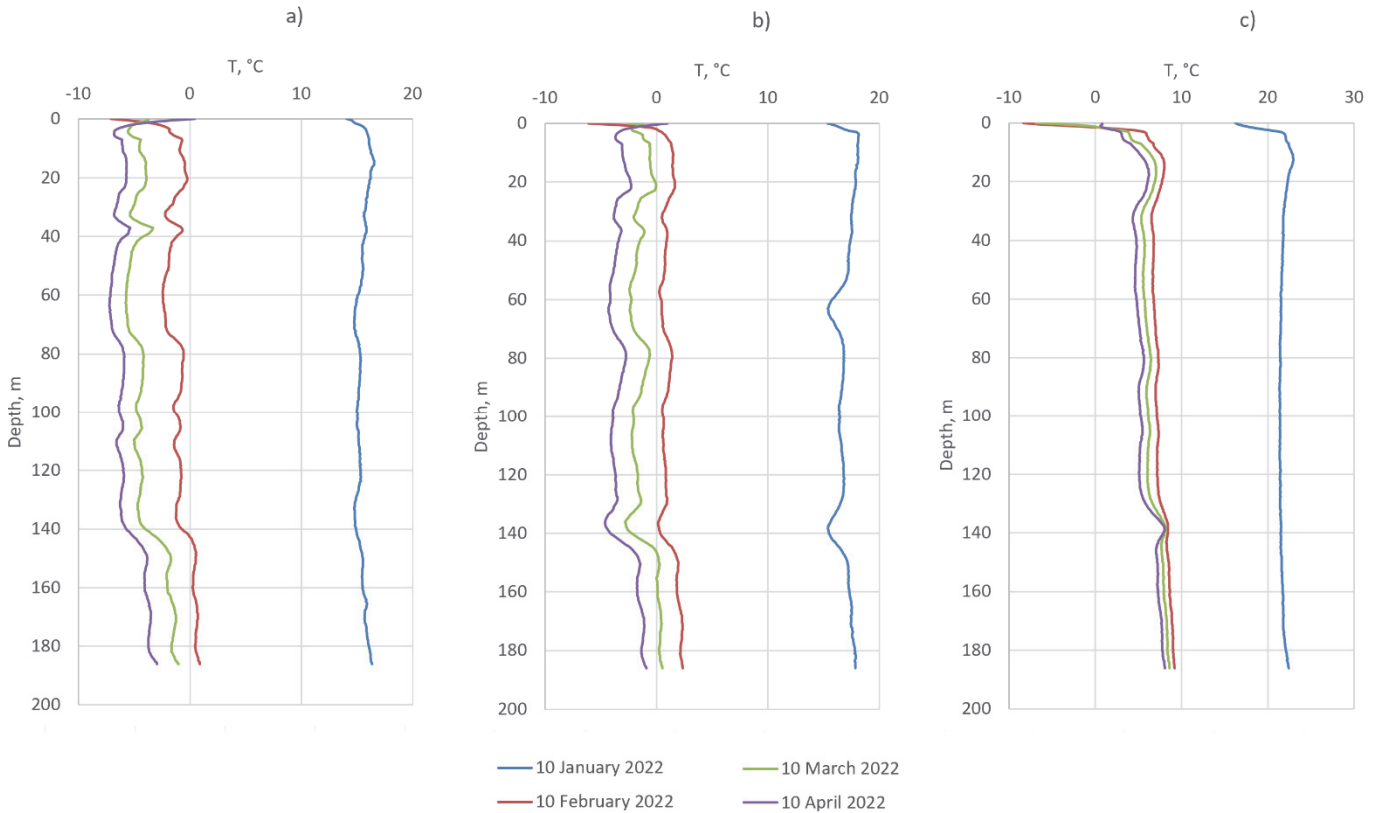
Figure 2: Experimental temperature distributions along the height of the various CT boreholes: a) CT-1, b) CT-2, c) CT-3.
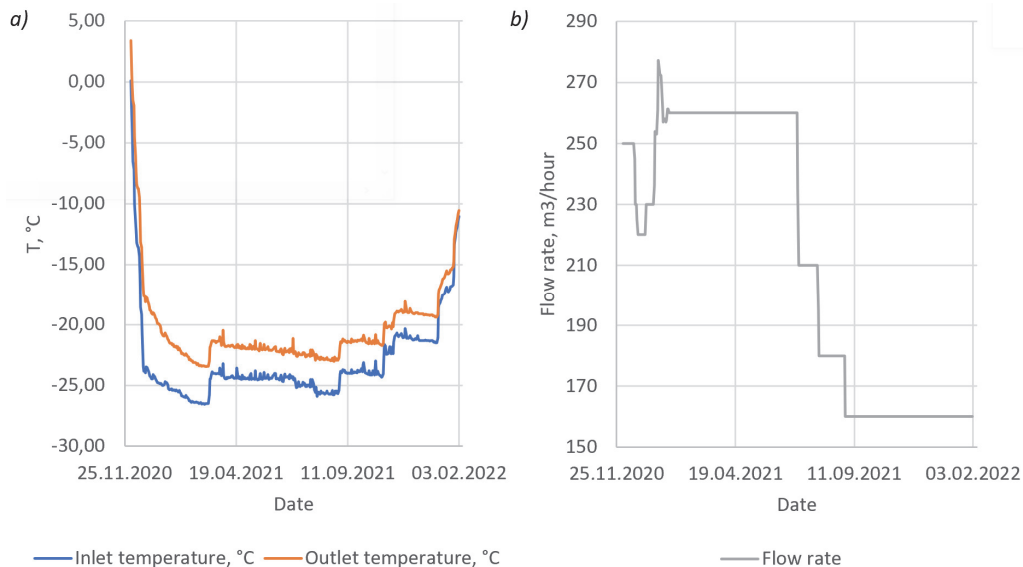
Figure 3: Time dependencies of the temperature (a) and total flow rate (b) in the brine pipe system.

INTERPRETATION OF THE TEMPERATURE FIELD

The available data from the experimental studies were used to adjust the parameters of the mathematical model of the frozen soil. The soil in the present study was a superposition of horizontal layers of soil with approximately uniform thermophysical properties. The horizontal soil layers had thicknesses of 10 m or greater. Regarding the middle horizontal sections of these soil layers, it was appropriate to accept the hypothesis of the smallness of vertical heat transfers and consider the heat transfer in the horizontal plane of each of the layers within the framework of the following mathematical model [20]:

$$\frac{\partial H(T)}{\partial t} = \left[\frac{1}{r} \frac{\partial}{\partial r} \left(\lambda r \frac{\partial T}{\partial r} \right) + \frac{1}{r^2} \frac{\partial}{\partial \varphi} \left(\lambda \frac{\partial T}{\partial \varphi} \right) \right] \tag{1}$$

$$\lambda = \lambda_{un} (1-i) + \lambda_{fr} i \tag{2}$$

$$H(T) = \begin{cases} \rho c_{un} (T - T_{lq}) + \rho_w nL, & T_{lq} \leq T \\ \rho_w nL \cdot (1-i), & T_{sd} \leq T < T_{lq} \\ \rho c_{fr} (T - T_{sd}), & T < T_{sd} \end{cases} \tag{3}$$

$$i(T) = \begin{cases} 1, & T < T_{sd} \\ (T_{lq} - T)/(T_{lq} - T_{sd}), & T_{sd} \leq T < T_{lq} \\ 0, & T_{lq} \leq T \end{cases} \tag{4}$$

$$\left[\lambda \frac{\partial T}{\partial N} - \alpha \left(T_{fb}(t) - T \right) \right] \Big|_{\Omega_{fb}} = 0 \tag{5}$$

$$T|_{\Omega_{out}} = T_0 \tag{6}$$

$$T|_{t=0} = T_0 \tag{7}$$

where H is the specific enthalpy of the soil, J/m³; r and φ are the polar coordinates, m; t is the physical time, s; λ_{un} and λ_{fr} are the mass thermal conductivities in the unfrozen and frozen zones, respectively, W/(m·°C); c_{un} and c_{fr} are the specific heat capacities of the soil in the unfrozen and frozen zones, respectively, J/(kg·°C); ρ is the soil density, kg/m³; T_{lq} is the temperature of the beginning of the pore water crystallization (liquidus temperature), °C; T_{sd} is the temperature of the beginning of the pore ice melting (solidus temperature), °C; i is the volumetric ice content of the soil, m³/m³; L is the specific heat of the crystallization of water, J/kg; n is the porosity of the soil; ρ_w is the pore water density, kg/m³; T_{fb} is the brine temperature in the freeze pipes, °C; T_0 is the temperature of the undisturbed soil at a distance from the freeze pipe contour, °C; α is the heat transfer coefficient at the freeze pipe walls, W/(m²·°C); $\Omega_{fb} = \cup \Omega_{fbi}$ are the boundaries with all the freeze pipes; Ω_{out} is the outer boundary of the simulation area; N is the coordinate along the normal to the boundary, m.

Accounting for the phase transitions of the pore water in this model was conducted by setting the specific enthalpy function (3). The jump of this function in the vicinity of the phase transition temperatures was determined by the value of the latent heat of the phase transition per unit volume of the soil. It was assumed that the temperature interval of this jump was sufficiently small compared to the characteristic temperature difference in the problem $T_0 - T_{fb}$. Thus, it was possible to consider the linear dependencies (2) and (4). In reality, the phase transition of the pore moisture for many soil layers can

occur in quite a wide temperature range, which is typically associated with the influence of the bound waters [21, 22] and the mineralization of the pore water [9].

The solution of the system of Eqns. (1) – (6) was conducted using the finite difference method in the Frozen Wall program developed at the Perm Mining Institute with the participation of the authors. The radius of the outer boundary of the computational domain for each of the layers was 51 m, and the radius of the freeze pipe was taken as 0.073 m. For the solution, a regular inhomogeneous mesh with thickening near the freeze pipes was used. An explicit first-order scheme in time and a second-order accuracy scheme (central difference) in space were used.

The initial values of all the thermophysical properties of the soil used in the calculations were taken based on laboratory studies of the soil samples. Tab. 1 shows the thermophysical properties used in the calculations for the three soil layers considered: sand, sandy clay and clay. Overall, there were 17 soil layers in the 185 m freeze interval. However, in this paper, we focus only on three of these layers.

Layer	Depth interval, m	T_0, °C	T_{lq}, °C	T_{sd}, °C	c_{fr}, J/(kg·°C)	c_{un}, J/(kg·°C)	ρ, kg/m³
Sand	2.1–18	9.5	-0.08	-1	908	1096	2110
Sandy clay	82.9-97.3	8.5	-0.07	-3	996	1131	2250
Clay	141.5-154.8	8.88	-0.68	-5	993	1259	2160

Table 1: Thermophysical properties of the considered soil layers.
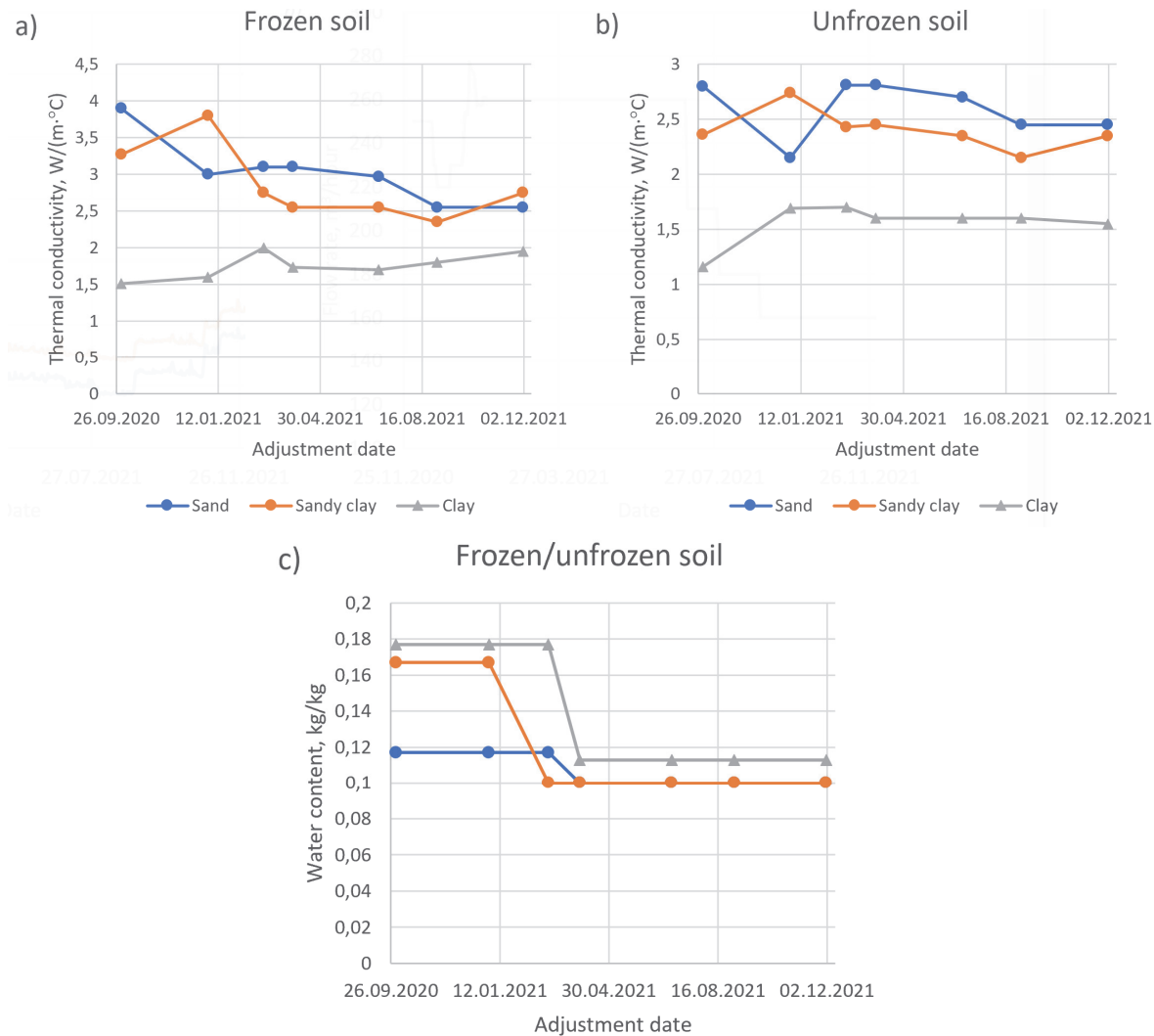
Figure 4: Dynamics of the effective thermophysical parameters of the soils during the model adjustments at various points in time: a) thermal conductivity of the frozen soil, b) thermal conductivity of the unfrozen soil, c) water content.

Furthermore, during the process of the experimental monitoring of the temperatures in the CT boreholes, the thermal model of each layer was parameterized. The model thermal conductivity and moisture content of the soil were adjusted according to the method [5, 18] to ensure the best match between the measured and calculated temperatures at the locations of the CT boreholes. Fig. 4 illustrates how the thermal conductivity and moisture of the soil were adjusted over time using three soil layers as an example. In this regard, the adjusted thermophysical properties in the model were no longer real, but some effective properties of the medium.

The calculated temperature profiles along the FW equidistant plane (see Fig. 1) [23] for the three considered soil layers and various time points are shown in Fig. 5. The zone r < 4 m is not displayed since it corresponds to the zone of the shaft under construction, and it was not considered when calculating the thickness of the FW. The horizontal dotted lines show the solidus temperatures that corresponded to the FW boundaries. The simulation time was counted from December 10, 2020. The total simulation time was 14 months. Fig. 5 shows that during the first 10 months, the temperatures of the soils generally decreased, the zone of negative temperatures expanded, and the thickness of the FW increased. After 10 months of freezing, there the temperature tended to increase, which was associated with the operation mode of the freezing station. The minimum temperatures on these curves were always higher than the temperature of the freezing brine, which was associated with the thermal resistance of the brine in the boundary layer near the pipe wall, the thermal resistance of the soils between the wall of the freeze pipe, and the FW equidistant plane.
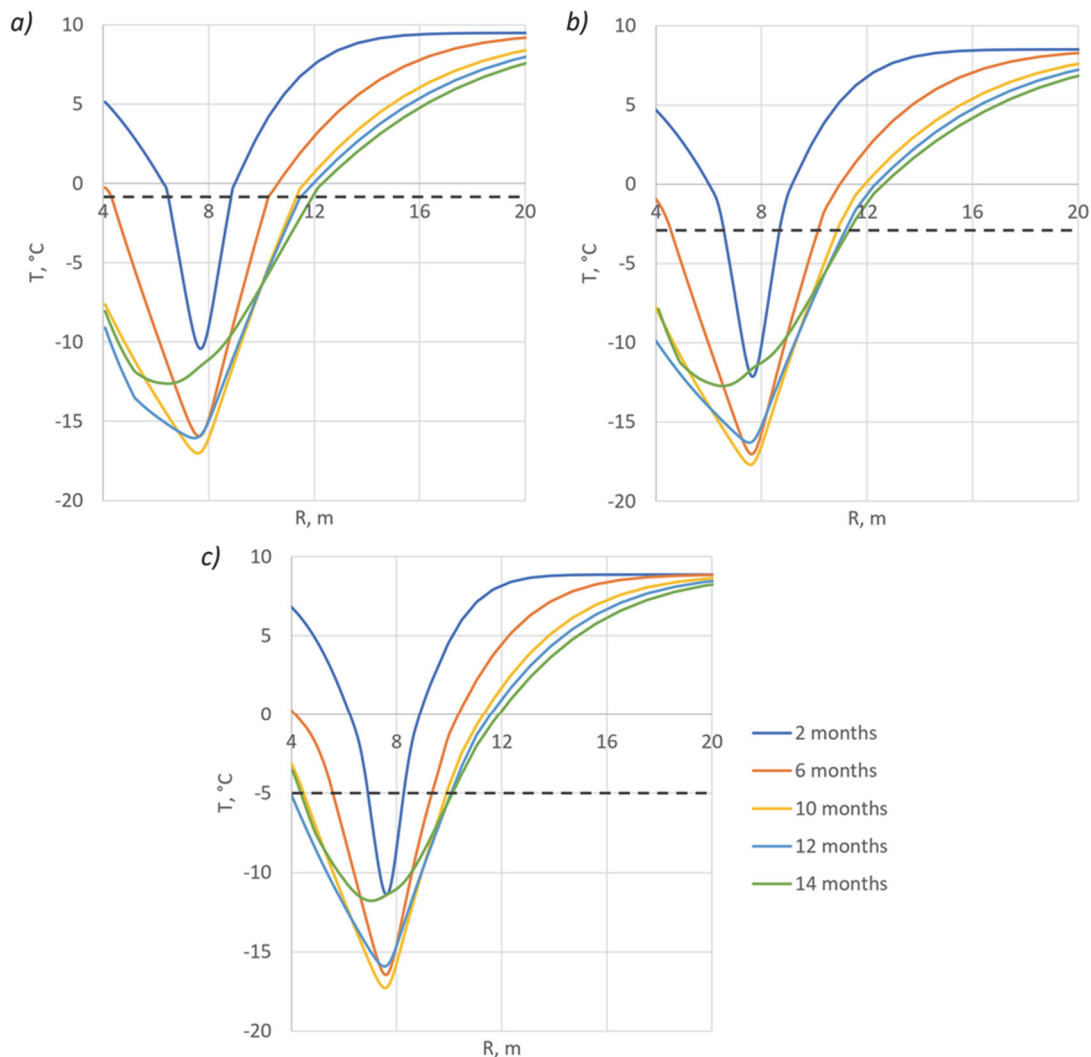
Figure 5: Radial temperature distributions along the FW equidistant plane.
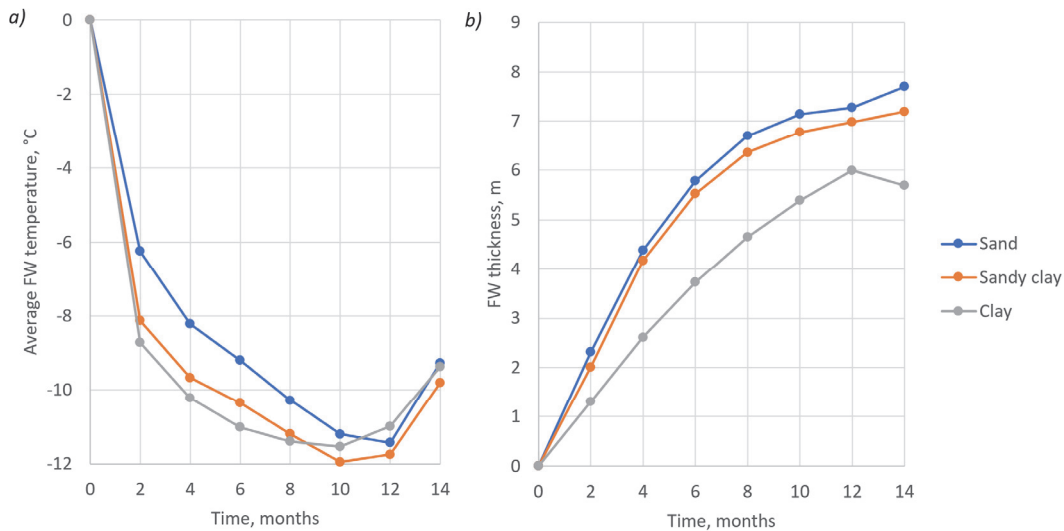
Figure 6: Time dependencies of the average temperature of the FW (a) and the thickness of the FW (b).

The radial dependencies showed a substantially inhomogeneous form. The temperature of the soils in the frozen zone varied over a wide range (sometimes exceeding 15°C). The average FW temperature during the considered time interval first decreased with time and, after 10 to 12 months, began to increase (see Fig. 6a).

The FW thickness for the sand and sandy clay continued to increase throughout the entire time interval, while the FW thickness of the clay increased up to 12 months and decreased in the interval from 12 to 14 months. This was because, for clay, the FW boundaries was considered to be at the lowest temperature of -5°C. This temperature is more difficult to maintain for the freezing system in the passive freezing mode. The model also considered that in the interval between 10 and 12 months, a mine shaft was constructed in the soil layers. This led to the heat inflows from the air space of the shaft. It is important to note that the increase in the average temperature of the FW began much later than the start of the ice holding stage, which was associated with the inertia of the thermal processes in the soil volume and the smoothness regarding the changing of the parameters of the freezing station. Only after the temperature of the brine in the freeze pipes became higher than -20°C, the average temperature of the FW began to increase.

MECHANICAL CALCULATION OF THE FW BEARING CAPACITY

The obtained temperature profiles were used to estimate the temporal change in the ultimate bearing capacity of the FW according to the strength criterion. Under the ultimate bearing capacity of FW, we mean the limiting value of the external lateral load, P, which the FW can withstand (see Fig. 7).
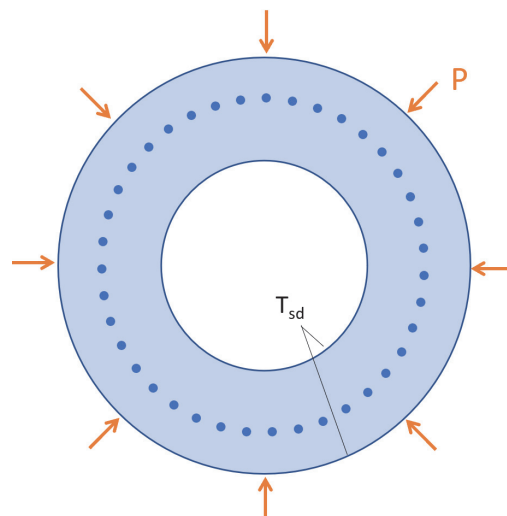
Figure 7: Schematic representation of the external lateral load, P, on the FW.

Let us use the expression relating the external load on the FW and its strength and geometric properties from [24]:

$$P = \frac{\overline{\Lambda}_{mean}}{\Lambda - 1}\varepsilon - \frac{\Lambda(\Lambda + 1)}{96(\Lambda - 1)^3}\Delta_c\varepsilon^3 \tag{8}$$

$$\varepsilon = \left(\frac{b}{a}\right)^{\Lambda - 1} - 1 \tag{9}$$

where a is the radius of the inner boundary of the FW, m; b is the radius of the outer boundary of the FW, m; P is the external lateral pressure, Pa; Δ_c is the difference between the maximum and minimum cohesion of the frozen soils in the FW with a non-uniform temperature distribution, Pa; Λ and $\overline{\Lambda}_{mean}$ are the coefficients in the linear Mohr-Coulomb law written with respect to the maximum σ_1 and minimum σ_3 principal stresses and a certain average temperature:

$$\sigma_1 = \Lambda\sigma_3 + \overline{\Lambda}_{mean} \tag{10}$$

$$\Lambda = \tan^2\left(\frac{\pi}{4} + \frac{\varphi_{mean}}{2}\right), \overline{\Lambda}_{mean} = 2c_{mean}\tan\left(\frac{\pi}{4} + \frac{\varphi_{mean}}{2}\right) \tag{11}$$

where c_{mean} is the frozen soil cohesion, averaged over the FW volume, Pa; φ_{mean} is the angle of internal friction, averaged over the FW volume, °.

In addition to formula (8), we also used the formula of S.S. Vyalov for the case of a finite height of an unfixed shaft wall, which was used in the Instructions for soil freezing at the Darasinsky mine:

$$E = \xi\frac{bP}{\sigma_c} \rightarrow P = \frac{\sigma_c E}{b\xi} = \frac{\sigma_c(b - a)}{b\xi} \tag{12}$$

where E is the FW thickness, m; σ_c is the strength of the frozen soils for uniaxial compression, Pa; b is the height of the unsupported shaft wall, m; ξ is the coefficient determined based on the nature of the pinching of the upper and lower ends of the FW.

The parameters a and b at different times can be determined based on Fig. 5 at the intersections of the corresponding temperature profiles using the solidus temperature line. The strength properties of the considered soil layers were taken from our previous work [8], in which the laboratory testing of soil samples for strength at various temperatures was conducted. The approximate linear functions of the limiting-long-term values of the strength properties of the soils on the temperature are presented in Tab. 2. These functions provided satisfactory results in the temperature range of -25 to -2°C. In formula (12), the strength of the frozen soils for the uniaxial compression was determined based on the average temperature of the FW. The height of the entry was assumed to be 5 m, and the coefficient was 1.73.

Layer	Cohesion, MPa	Tangent of the angle of internal friction, °	Uniaxial compressive strength
Sand	*0.814–0.121 T*	*0.436–0.0047 T*	*0.842–0.326 T*
Sandy clay	*0.729–0.117 T*	*0.304–0.0046 T*	*0.476–0.381 T*
Clay	*0.447–0.119 T*	*0.080–0.0072 T*	*1.095–0.276 T*

Table 2: Linear approximations of the temperature functions of the limiting-long-term values of the frozen soil strength properties.

We evaluated the bearing capacity of the FW in terms of the limiting value of the external lateral load that it can withstand under given thermophysical conditions obtained from the calculation using the model. Based on the available data on the

inhomogeneity of the FW temperature field, its geometric dimensions, and the strength properties of the soils, it was possible to calculate the time dependencies of the limiting value of the load on the FW using formula (8). The obtained time dependencies are shown in Fig. 8.
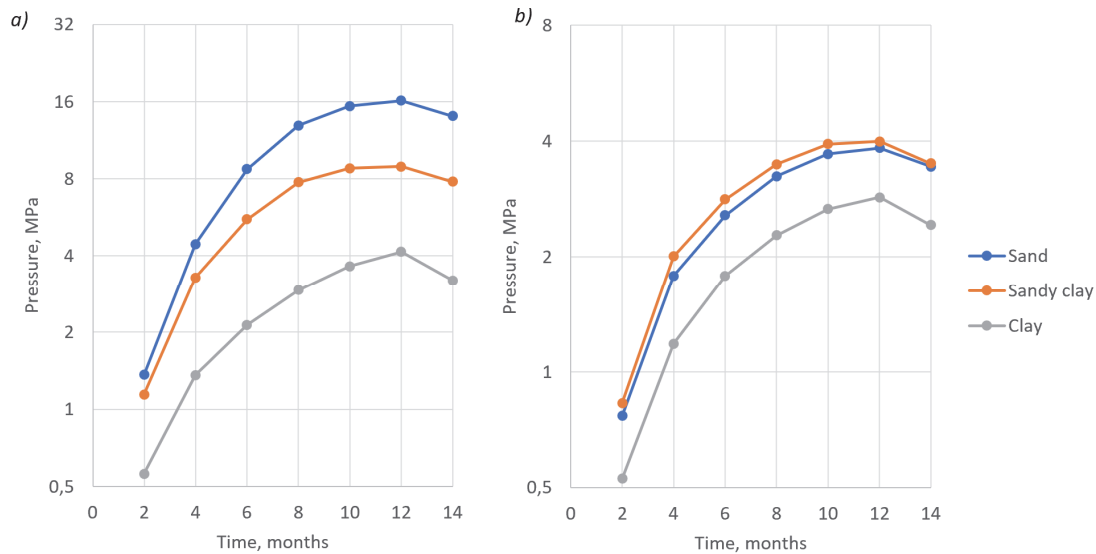
Figure 8: Time dependencies of the limiting value of the external lateral load that the FW can withstand

Fig. 8 shows that, in general, for 12 months, for all the considered soil layers, the FW strength increased. Simultaneously, the limiting values of the external load according to formula (8) were quite large and after four months exceeded the actual external load. For sand, the external load was 0.17 MPa, for sandy clay, it was 1.36 MPa, and for clay, it was 1.54 MPa. These values were calculated as the sum of two components: the lithostatic pressure and the pressure of the water column at the level of the bottom of each considered soil layer.

The limiting value of the external lateral load according to formula (12) was significantly lower, which was associated with the features of this formula and the physics included in it [25]. After only 6 months, this limiting value for the clay layer exceeded the actual external load that was calculated during the engineering and geological surveys and the development of the design documentation for the AGF (Fig. 8b).

In general, according to both formulas, the selected operation mode of the freezing station provided a significant margin for the required thickness of the FW during the construction period of the shaft. This was because when choosing the operating mode of the freezing station, the mine specialists were guided by other criteria:

− Maintaining the average temperature of the FW at a level of -8 to -10°C. It was for these temperatures that the design thicknesses of the FW were calculated.

− Sufficient freezing of the soils at a depth of 140 m, where the seepage flow of the pore water was revealed [20].

In addition to this, the analysis of the dynamic change in the FW bearing capacity presented in this paper was conducted after the construction of the skip shaft in the AGF interval of 0 to185 m. Moreover, the analysis conducted in the present study will be useful primarily for mine shafts that will be built in the future.

The data presented herein also did not account for the FW creep. The calculation of the required thickness of the FW according to the creep criterion is also mandatory in the design of the AGF [26, 27]. The calculated values of the FW thicknesses according to the creep condition for the relatively deep layers (sandy clay, clay) may be higher than the calculated values of the FW thicknesses according to the strength condition.

CONCLUSION

This paper describes a method for analyzing the dynamically changing bearing capacity of an FW according to temperature monitoring data. In the first stage, according to the temperature readings in the CT boreholes, the temperature field was interpreted throughout the entire frozen soil volume, and the actual FW thicknesses were determined from the soil freezing isotherms. Furthermore, the resulting temperature field was used to calculate the inhomogeneous distribution of the physical-mechanical and strength properties of the FW and determine the limiting value

of the external lateral load that the FW could withstand. This lateral external load was compared with the actual external load on the FW, which was determined from the design documentation for the AGF as the sum of the rock and hydrostatic pressures. The resulting time dependencies of the external lateral load on the FW can be used to optimize the operation mode of the freezing station at the ice holding stage.

ACKNOWLEDGEMENTS

REFERENCES

[1] Nicotera, M. V. and Russo, G. (2021). Monitoring a deep excavation in pyroclastic soil and soft rock. Tunnelling and Underground Space Technology, 117, 104130.

[2] Haß, H. and Schäfers, P. (2005). Application of ground freezing for underground construction in soft ground. In Proceedings of the 5th International Symposium TC28, Amsterdam, The Netherlands, pp. 405-412.

[3] Wu, T., Zhou, X., Zhang, L., Zhang, X., He, X. and Xu, Y. (2021). Theory and technology of real-time temperature field monitoring of vertical shaft frozen wall under high-velocity groundwater conditions. Cold Regions Science and Technology, 189, 103337.

[4] Pimentel, E., Papakonstantinou, S. and Anagnostou, G. (2012). Numerical interpretation of temperature distributions from three ground freezing applications in urban tunnelling. Tunnelling and Underground Space Technology, 28, pp. 57-69.

[5] Levin, L. Y., Semin, M. A. and Zaitsev, A. V. (2018). Solution of an inverse Stefan problem in analyzing the freezing of groundwater in a rock mass. Journal of Engineering Physics and Thermophysics, 91(3), pp. 611-618.

[6] Zhelnin, M. S., Plekhov, O. A., Semin, M. A. and Levin, L. Y. (2017). Numerical solution for an inverse problem about determination of volumetric heat capacity of rock mass during artificial freezing. PNRPU Mechanics Bulletin, (4), pp. 56-75.

[7] Zhang, B., Yang, W. and Wang, B. (2018). Plastic design theory of frozen wall thickness in an ultradeep soil layer considering large deformation characteristics. Mathematical Problems in Engineering.

[8] Semin, M.A., Brovka, G.P., Pugin, A.V., Bublik, S.A., Zhelnin, M.S. (2021). Effects of temperature field nonuniformity on strength of frozen wall in mine shafts. Mining Informational and Analytical Bulletin, 2021, 2021(9), pp. 79–93.

[9] Tounsi, H., Rouabhi, A., Tijani, M. and Guérin, F. (2019). Thermo-hydro-mechanical modeling of artificial ground freezing: application in mining engineering. Rock Mechanics and Rock Engineering, 52(10), pp. 3889-3907.

[10] Liu, Y., Li, K. Q., Li, D. Q., Tang, X. S. and Gu, S. X. (2022). Coupled thermal–hydraulic modeling of artificial ground freezing with uncertainties in pipe inclination and thermal conductivity. Acta Geotechnica, 17(1), pp. 257-274.

[11] Semin, M. A., Bogomyagkov, A. V. and Levin, L. Y. (2020). Theoretical analysis of frozen wall dynamics during transition to ice holding stage. Journal of Mining Institute, 243, pp. 319-328.

[12] Olkhovikov, Yu. P. (1984). Support of permanent openings of potash and salt mines. Publisher: Nedra, Moscow, Russia, 238 p. [In Rus]

[13] Marwan, A., Zhou, M. M., Abdelrehim, M. Z. and Meschke, G. (2016). Optimization of artificial ground freezing in tunneling in the presence of seepage flow. Computers and Geotechnics, 75, pp. 112-125.

[14] Huang, S., Guo, Y., Liu, Y., Ke, L. and Liu, G. (2018). Study on the influence of water flow on temperature around freeze pipes and its distribution optimization during artificial ground freezing. Applied Thermal Engineering, 135, pp. 435-445.

[15] Vitel, M., Rouabhi, A., Tijani, M. and Guérin, F. (2015). Modeling heat transfer between a freeze pipe and the surrounding ground during artificial ground freezing activities. Computers and Geotechnics, 63, pp. 99-111.

[16] Zueter, A., Nie-Rouquette, A., Alzoubi, M. A. and Sasmito, A. P. (2020). Thermal and hydraulic analysis of selective artificial ground freezing using air insulation: Experiment and modeling. Computers and Geotechnics, 120, 103416.

[17] Semin, M. A., Levin, L. Y. and Parshakov, O. S. (2020). Selection of working conditions and substantiation of operating mode of freezing pipes in maintenance of frozen wall thickness. Journal of Mining Science, 56(5), pp. 857-867.

[18] He, H., Dyck, M. F., Horton, R., Li, M., Jin, H. and Si, B. (2018). Distributed temperature sensing for soil physical measurements and its similarity to heat pulse method. Advances in agronomy, 148, pp. 173-230.

[19] Stutsel, B. M., Callow, J. N., Flower, K. C., Biddulph, T. B. and Issa, N. A. (2020). Application of distributed temperature sensing using optical fibre to understand temperature dynamics in wheat (triticum aestivum) during frost. European Journal of Agronomy, 115, 126038.

[20] Semin, M., Golovatyi, I. and Pugin, A. (2021). Analysis of temperature anomalies during thermal monitoring of frozen wall formation. Fluids, 6(8), 297.

[21] Kong, B., He, S., Xia, T. and Ding, Z. (2021). Research on Microstructure of Soft Clay under Various Artificial Ground Freezing Conditions Based on NMR. Applied Sciences, 11(4), 1810.

[22] Hou, S., Yang, Y., Cai, C., Chen, Y., Li, F. and Lei, D. (2022). Modeling heat and mass transfer during artificial ground freezing considering the influence of water seepage. International Journal of Heat and Mass Transfer, 194, 123053.

[23] Trupak, N. (1974) Ground Freezing in Underground Development. Nedra [In Rus.].

[24] Semin, M. (2021). Calculation of frozen wall thickness considering the non-uniform distribution of the strength properties. Procedia Structural Integrity, 32, pp. 180-186.

[25] Vyalov, S. S. (2013). Rheological fundamentals of soil mechanics. Elsevier.

[26] Vyalov, S. S., Zaretsky, Y. K. and Gorodetsky, S. E. (1979). Stability of mine workings in frozen soils. Engineering Geology, 13(1-4), pp. 339-351.

[27] Sanger, F. J. and Sayles, F. H. (1979). Thermal and rheological computations for artificially frozen ground construction. Engineering geology, 13(1-4), pp. 311-337.